





Article

Investigation of the Relationship between Topographic and Forest Stand Characteristics Using Aerial Laser Scanning and Field Survey Data

Botond Szász ^{1,*} , Bálint Heil ², Gábor Kovács ², Dávid Heilig ² , Gábor Veperdi ³, Diána Mészáros ², Gábor Illés ⁴  and Kornél Czímber ^{1,*} 

¹ Institute of Geomatics and Civil Engineering, Faculty of Forestry, University of Sopron, 9400 Sopron, Hungary

² Institute of Environmental and Nature Protection, Faculty of Forestry, University of Sopron, 9400 Sopron, Hungary; heil.balint@uni-sopron.hu (B.H.); kovacs.gabor@uni-sopron.hu (G.K.); heilig.david@phd.uni-sopron.hu (D.H.); meszaros.diana@uni-sopron.hu (D.M.)

³ Institute of Forest and Natural Resource Management, Faculty of Forestry, University of Sopron, 9400 Sopron, Hungary; veperdi.gabor@uni-sopron.hu

⁴ Forest Research Institute, University of Sopron, 9600 Sárvár, Hungary; illes.gabor@uni-sopron.hu

* Correspondence: szasz.botond@uni-sopron.hu (B.S.); czimber.kornel@uni-sopron.hu (K.C.)

Abstract: The article thoroughly investigates the relationships between terrain features and tree measurements derived from aerial laser scanning (ALS) data and field surveys in a 1067-hectare forested area. A digital elevation model (DEM) was generated from ALS data, which was then used to derive additional layers such as slope, aspect, topographic position index (TPI), and landforms. The authors developed a mathematical procedure to determine the radii for the topographic position index. The canopy height model was created, and individual trees were segmented using a novel voxel aggregation method, allowing for the calculation of tree height and crown size. Accuracy assessments were conducted between ALS-derived data and field-collected data. Terrain variability within each forest unit was evaluated using characteristics such as standard deviation, entropy, and frequency. The relationships between tree height and the derived topographic features within forest subcompartments, as well as the correlation between the height yield map for the entire area and the TPI layer, were analysed. The authors found strong correlation between the topographic position index and tree heights in both cases. The presented remote-sensing-based methodology and the results can be effectively used in digital forest site mapping, complemented by field sampling and laboratory soil analyses, and, as final goal, in carbon stock assessment.

Keywords: LiDAR; ALS; topography; orography; dendrometry; tree height relationships; site mapping



Citation: Szász, B.; Heil, B.; Kovács, G.; Heilig, D.; Veperdi, G.; Mészáros, D.; Illés, G.; Czímber, K. Investigation of the Relationship between Topographic and Forest Stand Characteristics Using Aerial Laser Scanning and Field Survey Data. *Forests* **2024**, *15*, 1546. <https://doi.org/10.3390/f15091546>

Academic Editor: Jianping Wu

Received: 30 July 2024

Revised: 30 August 2024

Accepted: 31 August 2024

Published: 2 September 2024



Copyright: © 2024 by the authors. Licensee MDPI, Basel, Switzerland. This article is an open access article distributed under the terms and conditions of the Creative Commons Attribution (CC BY) license (<https://creativecommons.org/licenses/by/4.0/>).

1. Introduction

Due to climate change, Hungarian/European forests are undergoing rapid and significant changes, with notable fluctuations in the water balance. Both underground and aboveground carbon storage are affected, as well as the role of forests in mitigating the effects of climate change. The currently used methods for site and carbon stock determination are not yet suitable for tracking these rapid changes. Furthermore, only 12% of the Hungarian forest database contains up-to-date site data based on direct site-specific investigations. Therefore, there is an urgent need for more effective and accurate assessment and monitoring of environmental and ecological conditions. The main motivation for this interest is the potential to lower costs and achieve more precise and efficient assessments of forest characteristics.

To develop the aforementioned modern methodology, the SoilSense project was launched in connection with the Hungarian Climate Change Action Plan. It started in the fall of 2023 with the support of the Hungarian Ministry of Agriculture. The methodology

to be developed uses surface models generated from point clouds obtained through aerial laser scanning (ALS), individual tree data, and forest stand and soil characteristics collected in the field. This approach aims to refine forest site mapping and determine carbon stock [1]. This is important because precise site mapping and forest inventory play an important role in European forestry.

The ultimate goal is to create an accurate site map from the above data, determine the aboveground and belowground carbon stocks, and develop a modern, cost-effective, objective, repeatable, and detailed site mapping methodology that combines remote sensing with field sampling, applicable to forests both in Hungary and all over Europe. The developed method can support stakeholders and policy makers in forest management decisions to mitigate the effects of climate change.

The project is expected to last 3 years. Among the project's milestones, the first focuses on establishing the model area, acquiring remote sensing databases, and developing the soil survey methodology. The second milestone involves field surveys and the processing of remote sensing data. The third milestone pertains to the laboratory processing of soil samples and the production of reference data, while the fourth milestone involves model development and validation.

In this article, we aim to report on the establishment of the research area, the processing of aerial laser scanning data, and the comparison of the obtained data with field data. From the laser scanning, we generated an elevation model and a canopy height model, segmented the point cloud into individual trees, and compared it with the circular plot field survey data.

A digital elevation model (DEM) is typically in a raster (regular grid) format, less frequently a vector (irregular triangular network) format, representing the elevation of the Earth's surface. It provides fundamental information about the terrain surface [2]. From the digital elevation model, one can derive slope, aspect, hydrological models, topographic index, and many other useful thematic layers [3]. The slope indicates the rate of elevation change based on the adjacent 4 (or 8) pixels, while the aspect shows the direction of the steepest descent, measured in degrees clockwise from north [4].

By analysing these derived models, information can be obtained about the study area, such as flow direction [5] and outflow points from the area [6], as well as the distribution of landforms [7]. One of the most important characteristics of a DEM is its spatial resolution, which indicates the area covered by one pixel on the ground. The spatial resolution significantly affects the results of various terrain model analyses, whether it is slope [8], aspect, or even a hydrological model [9–11].

Orography, also known as mountain geography, is a branch of physical geography that deals with geological formations, primary and secondary landforms, the surface characteristics of mountains and hills, and their descriptions [12]. Analysing the topographic position index (TPI) is one possible solution for deriving various orographic features.

The topographic position index (TPI) compares the elevation of individual pixels with the average elevation of surrounding pixels within a specified shape (circle, square). Positive TPI values describe points on the terrain that are higher than their surroundings, while negative values indicate the opposite [13]. The classification also considers the slope associated with the given pixel. If the TPI value is significantly less than zero, it typically represents a valley floor (or an area close to one). If the TPI value is close to zero, it could indicate either a flat area or a moderate, open slope; the slope is used to differentiate between these two possibilities [14].

A key aspect of TPI analysis is selecting the appropriate search radius. For example, with a smaller radius, a valley floor's slight prominence will be clearly defined, but with a larger radius, it may not appear. Conversely, a narrower watershed located on a ridge might not be identifiable with a larger radius, while a smaller radius would only detect the hill or watershed itself without providing information about its broader context. To address this, TPI analysis should be performed using two different radii. By combining the results from these radii, a total of 10 distinct landform types can be distinguished [14]. In

this case, the goal is to determine the two radius values that are suitable for categorising landforms at the scale required for site mapping.

An important aspect of applying aerial laser scanning (LiDAR) in forestry is the selection and interpolation of elevation points beneath the forest canopy. Strip-based elevation point selection and averaging were performed by [15]. Recently, several adaptive triangulated irregular network (TIN) fitting methods have been developed [16,17], which filter LiDAR elevation points and produce a vector surface model. Elevation points can also be filtered from LiDAR point clouds using various methods, such as slope filters [18] or morphological filters (combining minimum and maximum filters) [19,20]. Multi-level curvature analysis is another effective method for point selection [21]. Meng et al. [22] give an overview of LiDAR terrain modelling methods. It is also important to mention the latest clothing simulation algorithms [23,24].

Another critical aspect of processing laser scanned data in forested areas is the generation and segmentation of the canopy height model (CHM) to identify individual trees. Early methods sought local maxima in the canopy height model [25,26]. Popescu et al. [27] introduced a tree-height-dependent variable window size to filter nearby local maxima. Morsdorf et al. [28] conducted pine identification. Chen et al. [29] utilised a canopy maxima model based on smoothing the canopy surface maximum and inverse watershed method. Koch et al. [30] employed an inverse watershed. Hyyppä et al. [31] applied region growing. Later, procedures operating directly on 3D point clouds emerged. Lee et al. [32] developed adaptive k-means clustering for tree segmentation. Ferraz et al. [33] used 3D adaptive mean-shift segmentation in multi-layered Mediterranean forests. Li et al. [34] published a top-down region growing approach. Kaartinen et al. [35] and Jakubowski et al. [36] compared available individual tree detection methods. Strimbu V. and Strimbu B. [37] developed graph-based segmentation. Duncanson et al. [38] used multi-layered crown delineation. Yang et al. [39] employed a hierarchical minimum cut approach. Lindberg and Holmgren [40] also reviewed available methods. Hu et al. [41] advanced recognition techniques. Ayrey et al. [42] introduced layer stacking recognition. Wan Mohd Jaafar et al. [43] further improved watershed and segmentation procedures. Wang et al. [44] used a method based on a Gaussian distributed regional growth algorithm and Voronoi range constraints to extract street tree geometries from vehicle-mounted LiDAR point clouds. Czimmer [45] developed a voxel aggregation method for detecting the canopies of broadleaf trees.

There are also studies which were looking for a connection between topography and forest stand parameters, especially tree height. McNab [46] found out that the geometric shape of the land surface (terrain shape index) is highly correlated with total height of trees in the southern Appalachians. Tateno and Takeda [47] showed that the maximum tree height is greater on the lower part, and the crown closure increased up the slope in a cool-temperate deciduous broadleaved forest in Japan. Rahman et al. [48] proved that canopy height is greater by 5–10 m in the concave valleys than on the convex slopes and ridges in central Japan. Bałazy et al. [49] also showed that tree growth dynamics are largely dependent on local topographic conditions but found out that the role of TPI is relatively small.

2. Materials and Methods

2.1. Introduction of the Project Area

The project's study area is the Dudlesz Forest, located on approximately 1067 hectares to the north of Sopron, Hungary (Figure 1). Geographically, it belongs to the Fertőmelléki Hills, a young Miocene sedimentary rock landscape characterised by a gently undulating, low-relief, denudational–erosional hill range. Its climate is moderately cool and moderately dry. The potential vegetation types include hornbeam–oak forests and sessile oak forests, but due to the geological conditions, there are also significant edaphic forest communities present. The region is almost entirely covered by Rendzic Leptosols and Cutanic Luvisols or Cambisols [50].

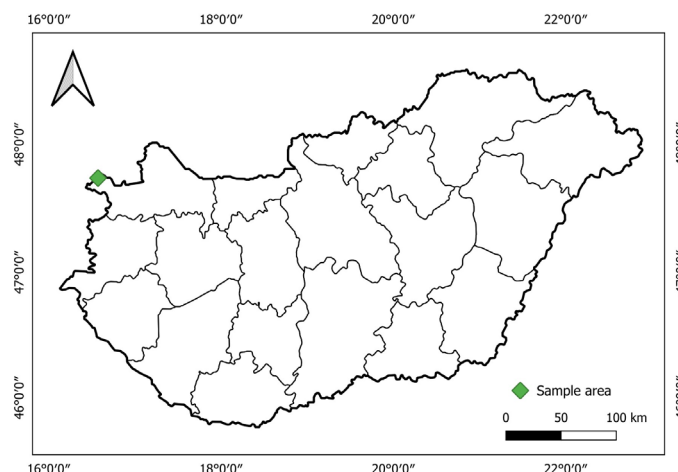


Figure 1. Location of Dudlesz Forest in Hungary.

2.2. Laser Scanning

For the creation of surface models, the point cloud was provided by EnviroSense Ltd. (registered in Debrecen, Hungary), surveyed using LiDAR technology with a Riegl V780 II sensor (manufactured by RIEGL Laser Measurement System GmbH, Horn, Austria) from a small aircraft under leafless conditions, in 2023. The provided point cloud has an average point density of 20 points/m², from which the digital surface model (DSM), the digital elevation model (DEM), and the normalised surface model (nDSM) were derived by subtracting the latter from the former, or, in this case, given that it is a forested area, the canopy height model (CHM).

To create the elevation model, we used the TreeDetect (v.1.24.5.10) software (by TopoLynx Ltd., registered in Kőszeg, Hungary), which is specifically developed for processing aerial laser scanning data of forested areas [45]. The software's algorithms generate raster surface models and vector single-tree data (stem points and crown polygons). In the first phase of the complex processing, the software filters out scattered low points, selects elevation points using a hierarchical morphological method, and interpolates them to create the digital elevation model (DEM). In the second phase, the software filters out scattered high points, selects canopy height model (CHM) points, and performs CHM interpolation and export. In the third phase, TreeDetect employs a specialised voxel aggregation algorithm to segment individual tree canopies. The key parameters of the processing are the voxel size, the voxel aggregation ranges for stem and crown detection, and single-tree segmentation parameters. This method is comparable to the layer stacking method and is particularly advantageous for broadleaved trees, where the canopy surface shows minimal height variation within the stand. By examining the canopy in depth using voxels, the boundaries between individual tree canopies are clearly delineated.

2.3. Thematic Layers Derived from the DEM

The digital elevation model (DEM) generated from the point cloud and the thematic layers derived from it have a spatial resolution of 1 m/pixel. As this resolution falls into the category of high-resolution, detailed models, it can capture even minor features such as small depressions, pits, cones, and forest roads, which are not relevant in site mapping due to their small size. Therefore, it was necessary to apply a Gaussian filter ($r = 10$ m, $s = 100$) to remove these micro-relief features, which was performed using QGIS software (v.3.26.2) (Figure 2). We ran slope and aspect analyses on the smoothed elevation model, also using QGIS. The calculation of the topographic position index (TPI) was performed using an algorithm developed by us.

Naturally, each pixel is associated with a slope and an aspect value. However, for easier interpretation and visualisation, we categorised these continuous values: for slope, we used a 5-degree resolution, while for aspect, we distinguished 8 categories based on

the 4 cardinal and 4 intercardinal directions. In both cases, areas with a slope of less than 2 degrees were considered flat.

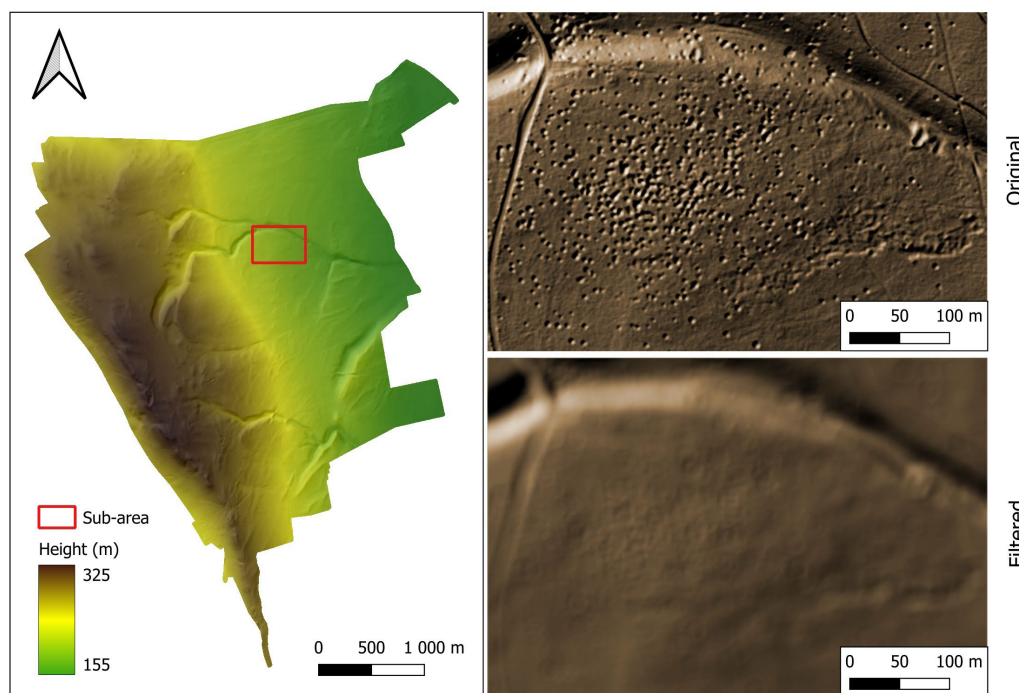


Figure 2. Illustration of Gaussian Filtering on a sample area.

To determine the appropriate radii for the TPI analysis, we initially ran the algorithm with several radius values. These values were chosen based on the DEM resolution (1 m/pixel): starting with five times the resolution and its multiples (i.e., between 5 and 25 m, in 5 m increments), and then three, four, and five times those values (for example, for a 15 m radius, this included 45, 60, and 75 m), resulting in a total of 14 TPI models.

We calculated the standard deviation using focal statistical analysis with a 25 m radius for these models. The global maxima of the resulting standard deviation rasters were plotted on a graph, and a second-order polynomial trendline was fitted. The TPI value closest to the maximum point of the curve provided the larger radius value, while the smaller radius value was selected based on the point where the tangent line intersects the origin. Using these two selected radius values, we classified the pixels into 10 topographic categories (Table 1).

Table 1. Landform categories [14].

ID	Landform Names	Small Radius TPI	Large Radius TPI	Slope
1	Canyons, Deeply Incised Streams	$TPI \leq -1$	$TPI \leq -1$	
2	Midslope Drainages, Shallow Valleys	$TPI \leq -1$	$-1 < TPI < 1$	
3	Upland Drainages, Headwaters	$TPI \leq -1$	$TPI \geq 1$	
4	U-shaped Valleys	$-1 < TPI < 1$	$TPI \leq -1$	
5	Plains	$-1 < TPI < 1$	$-1 < TPI < 1$	$\leq 2^\circ$
6	Open Slopes	$-1 < TPI < 1$	$-1 < TPI < 1$	$> 2^\circ$
7	Upper Slopes, Mesas	$-1 < TPI < 1$	$TPI \geq 1$	
8	Local Ridges/Hills in Valleys	$TPI \geq 1$	$TPI \leq -1$	
9	Midslope Ridges, Small Hills in Plains	$TPI \geq 1$	$-1 < TPI < 1$	
10	Mountain Tops, High Ridges	$TPI \geq 1$	$TPI \geq 1$	

After creating the three rasters and categorising them, we examined the standard deviation of elevation and slope angle at the forest subcompartment level. Addition-

ally, we assessed the extent of areas classified into different categories and derived the following metrics:

1. Frequency: The area proportion of the largest category;
2. Stability: The difference in area proportions between the largest and the second largest categories;
3. Shannon Entropy, calculated as [51]:

$$H(S) = -1 * \sum_{i=1}^n P_i * \log_2 P_i \quad (1)$$

where P_i is the relative frequency (the area of the given category/the total area of the forest subcompartment). We then examined any potential correlations both within a single thematic layer and between different thematic layers.

We established 272 field points on the site, whose centre points were surveyed using GNSS RTK technology (with FORGEO Puli GNSS receiver and Corrigio RTK correction service, Baja, Hungary) and then marked. We assessed the trees within a 12.61 m radius around each field point (500 m² sample areas). For each tree, we recorded the species, diameter at breast height (DBH) with a caliper, height using a trigonometric height meter (Nikon Forestry Pro, manufactured by Nikon, Tokyo, Japan), and distance from the middle of the sample area with an ultrasonic distance meter (Vertex III, manufactured by Haglöf, Långsele, Sweden). We also documented standing and lying deadwood within the sample points.

We compared the field measurements with the LiDAR-derived layers (DEM and CHM) and examined the relationships between tree heights, the topographic model, and derived themes, particularly the topographic position index (TPI). Firstly, within a forest stand (15B) that traverses a deeper valley, we created a height increment map by using tree heights derived from the CHM and the age ratio of the tree stands recorded in the forest stands. We analysed the resulting map data by TPI groups.

The processing steps described above are illustrated in Figure 3 flowchart.

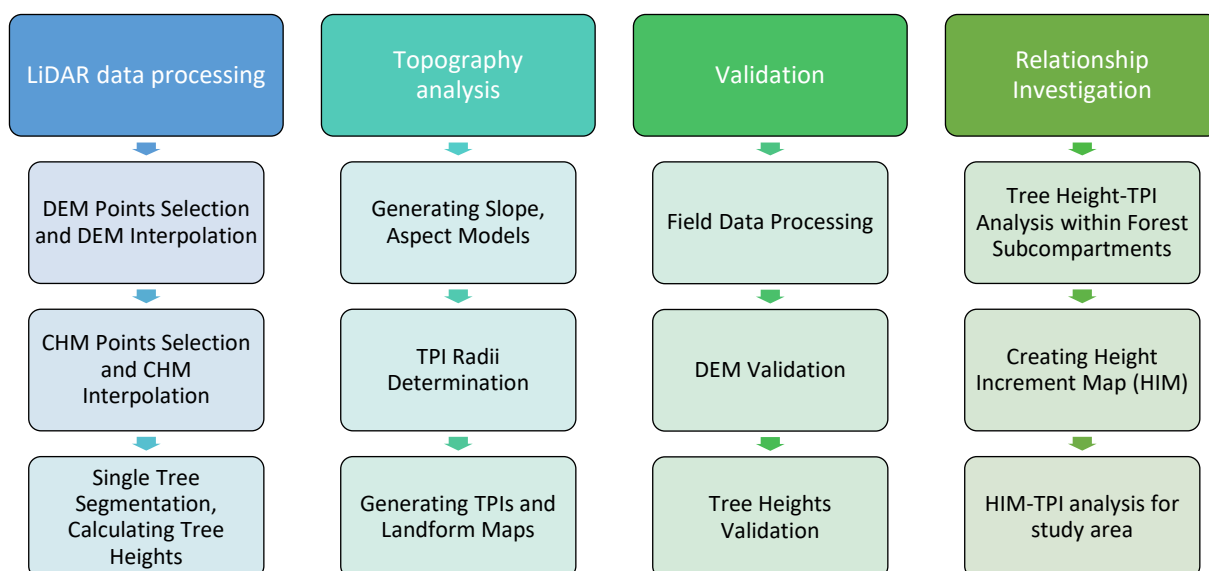


Figure 3. Flowchart of the processing steps.

3. Results and Discussion

DEM

We performed the verification of the digital elevation model at the centres of the field points. We compared the elevation of the 272 point centres with the interpolated elevation model derived from the LiDAR data. The average difference between the two elevation

datasets was 1 cm, with a standard deviation of 6 cm, which is considered very good for a forested area, especially given the presence of coniferous stands, including Scots pine and black pine species.

a. Derived layers

After the creation and categorisation of the slope and aspect rasters, the determination of the two radius values required for the TPI analysis is illustrated in Figure 4.

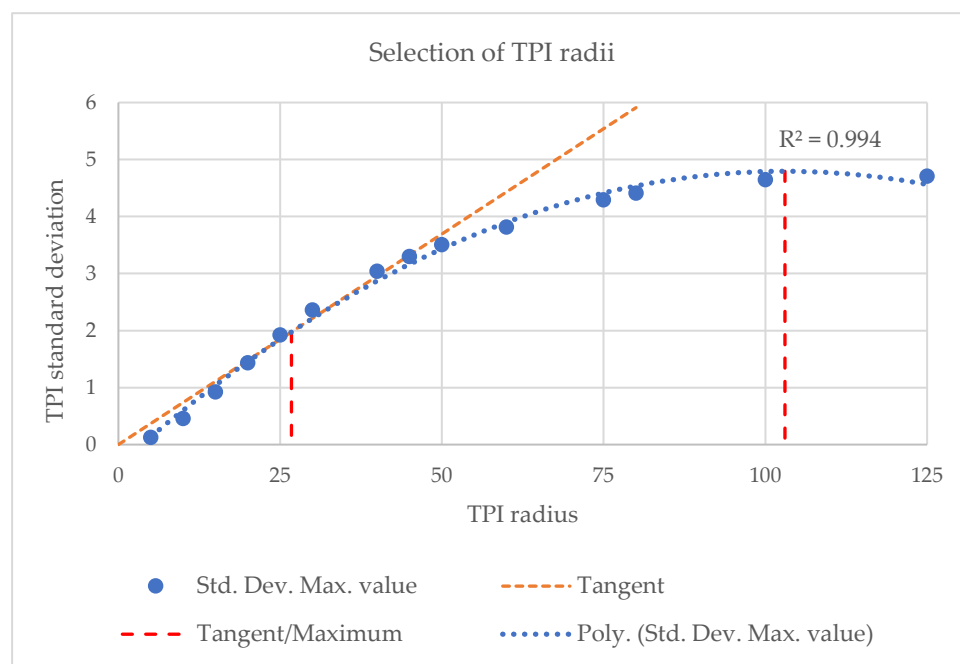


Figure 4. Selection of TPI Radius Values.

It can be seen that the second-degree polynomial curve fitted to the maximum deviation peaks at a radius of 100 m (more precisely, 103.03 m), while the tangent line passing through the origin touches the curve near a radius of 25 m (more precisely, 26.75 m). Rounding was necessary both due to the raster's rounded metre resolution and to enhance clarity. Additionally, the multiplier between the applied radii was considered as an integer value. Thus, the smaller TPI analysis radius was set to 25 m, and the larger radius to 100 m, with a factor of four between them.

The original digital elevation model and the three derived thematic layers are illustrated in Figure 5.

Figure 5 shows that a large portion of the study area falls into the “Open Slope” category (59.90%), where the predominant aspects are to the northeast and east, with slopes ranging from 2°–10°. Steeper slopes are found along the deep valleys that cut through the area (where the aspect varies significantly) and along the western edge, where the southwestern aspect is most prominent. The valley bottoms are characterised by category 1 (Canyons, Deeply Incised Streams: 0.96%), while the slopes are categorised as 4 (U-shaped Valleys: 13.23%). In addition, significant areas fall into category 7 (Upper Slopes, Mesas: 15.16%) and category 5 (Plains: 9.38%). Category 10 (Mountain Tops, High Ridges: 1.20%) is also notable, representing ridges mainly found along the western edge of the area. The remaining four categories are present only in negligible proportions and are dispersed throughout the area.

Figure 6 illustrates the variation in elevation above sea level, slope angle, and the 25 m radius TPI for each forest subcompartment. This is a method for characterising the variability within each spatial unit using the yet-to-be-categorised statistical rasters.

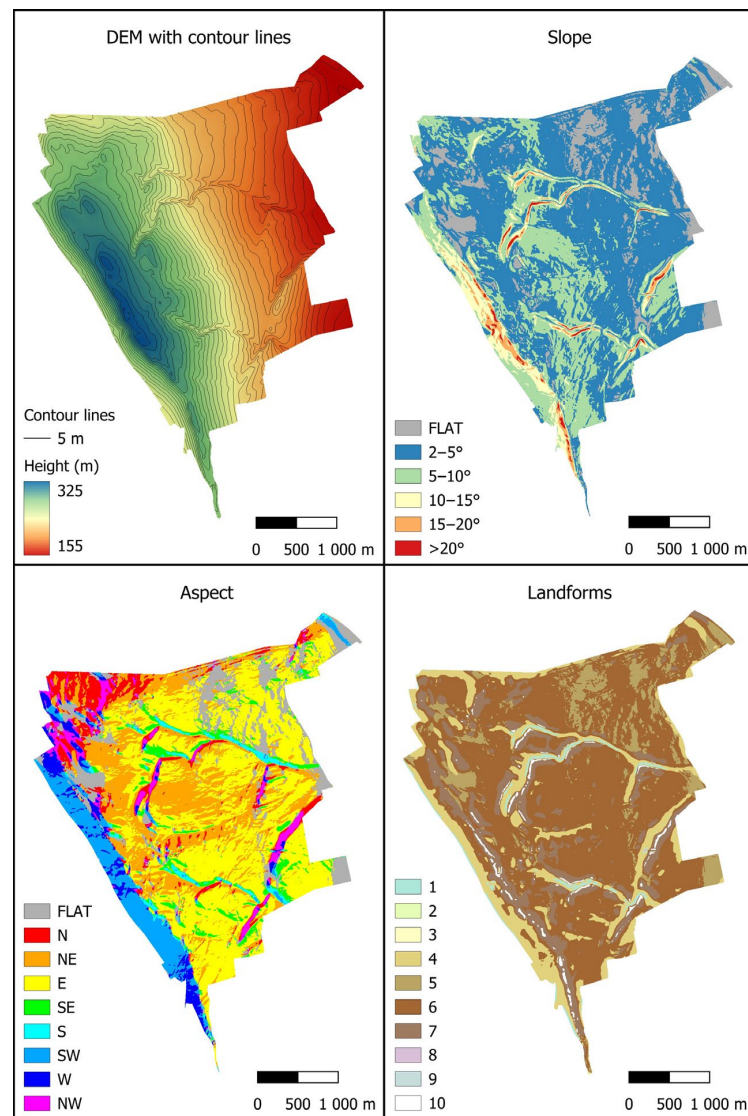


Figure 5. Categorized DEM and Derived Thematic Layers.

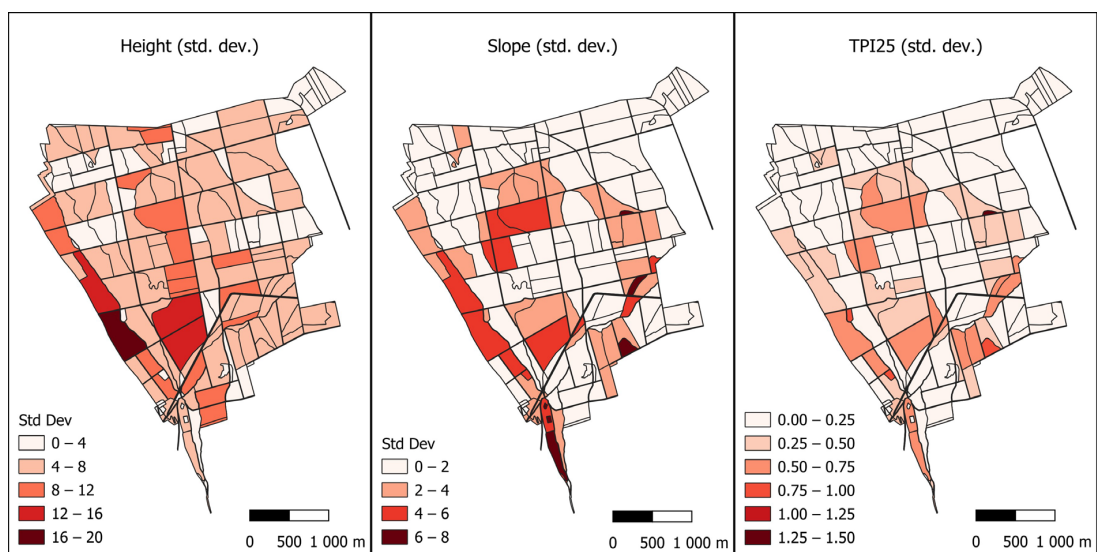


Figure 6. Variation of Elevation, Slope, and TPI25 by forest subcompartment.

Among these, we identified a relationship between slope and TPI25, illustrated by the graph in Figure 7.

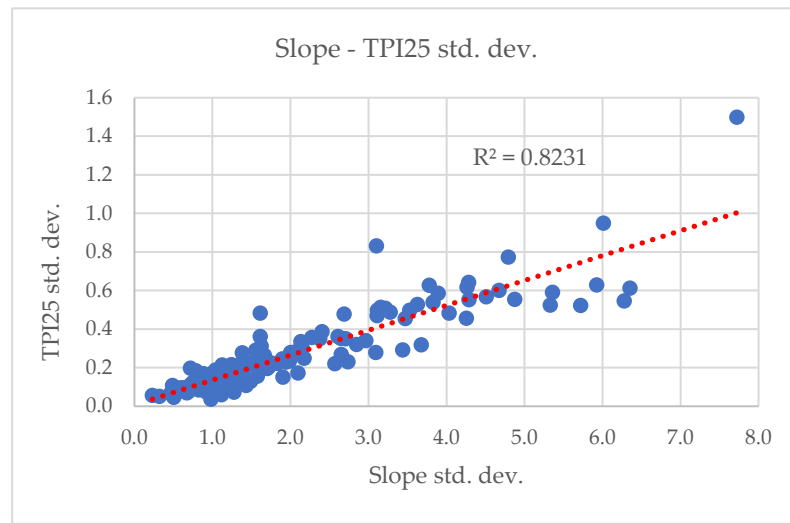


Figure 7. Relationship between slope and TPI25 standard deviation by forest subcompartment.

After categorising the three thematic layers, we examined the relationships between frequency, stability, and entropy, which are illustrated in Figure 8 with respect to topographic categories. A second-order polynomial relationship was established between frequency and entropy. Observing the graph, moving backward along the x-axis (frequency), a sudden jump is noted toward lower entropy values on the y-axis. This jump occurs because, beyond this point, no category is in absolute majority, leading to increased variability (Figure 8a). When weighting frequency by stability, the trendline becomes more linear. However, as it approaches the y-axis, deviations increase significantly, resulting in a lower R² value (Figure 8b).

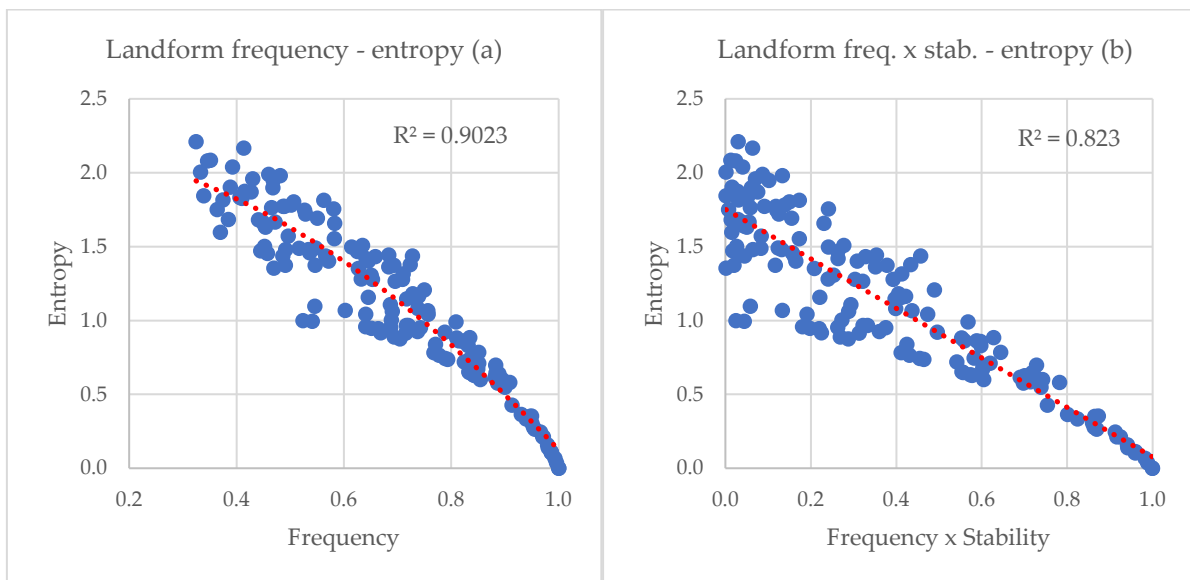


Figure 8. Entropy of topographic categories by forest subcompartments as a function of frequency and frequency weighted by stability.

We were also interested in exploring any potential correlations between the three entropy layers in terms of variability. The entropy of these themes by forest subcompartments is illustrated in Figure 9.

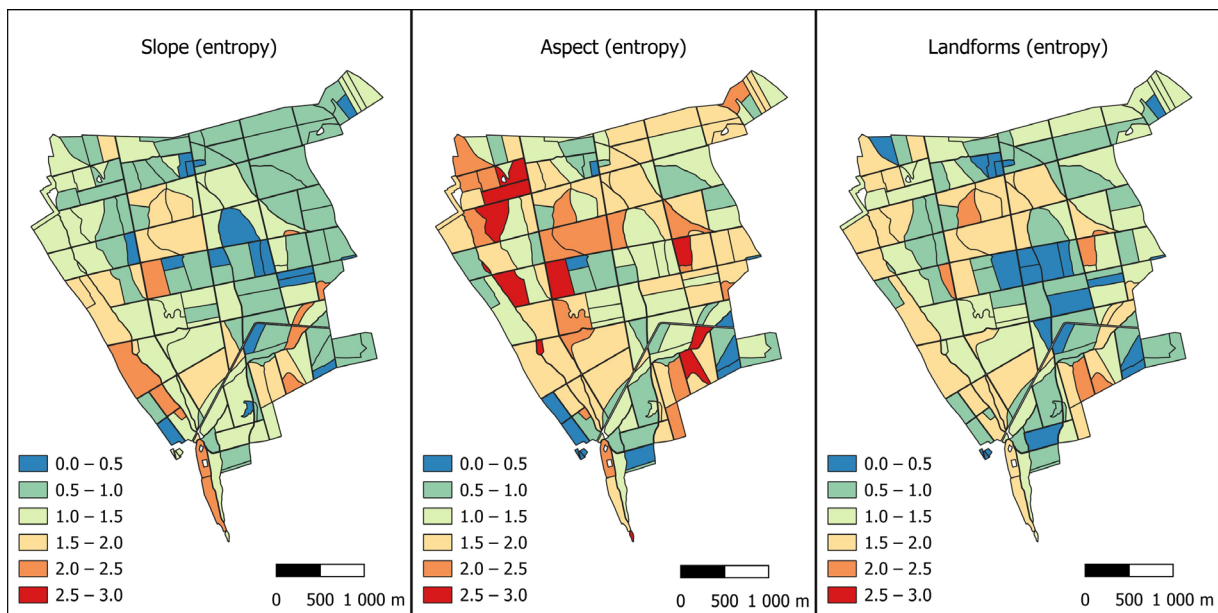


Figure 9. Three entropy layers by forest subcompartments.

The graphs shown in Figure 10 reveal that neither slope (Figure 10a) nor aspect (Figure 10b) resulted in a convergent trend line when compared with landform types. The R^2 value is around 0.5 in both cases, and visually, it is evident that there is considerable dispersion in the data, indicating that there is no clear correlation between the variability of the three themes.

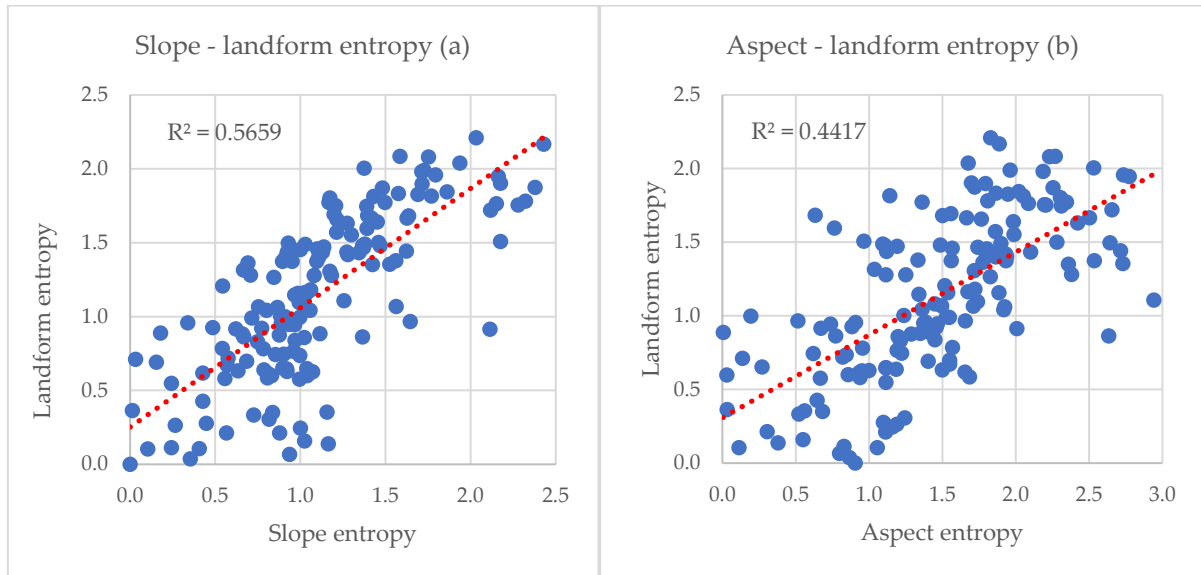


Figure 10. The relationship between the entropy of slope, aspect, and the entropy of landforms within forest subcompartments.

b. Tree height comparison

After a detailed analysis of the topography and derived thematic layers, we compared the tree heights measured at the 272 field survey points with those obtained from LiDAR data. For each survey point, we compared the average tree height measured in the field with the average height of tree segments identified in the LiDAR data within the area of the survey point. Before comparison, we filtered out significant errors, such as cases where field height measurements were not taken in areas undergoing reforestation or in dense

juvenile stands, or where only the height of residual trees was measured. After filtering, the difference in average height between individual trees was -0.13 m, with a standard deviation of 1.52 m.

We found a clear correlation between TPI values and tree heights obtained from LiDAR point cloud segmentation in areas where the 25 m radius TPI is negative, indicating the area is identified as a local catchment. These areas are the west–east-oriented valleys in the centre of the sample area, which are approximately 20–40 m wide and 3–8 m deep. The results are well illustrated within a forest subcompartment (Figure 11), where the trees are of the same age, but their heights differ. In the valleys, the average tree height is 22.74 m, while in the flat areas it is 18.81 m. In the figure, valleys marked in a dark color contain taller trees marked in blue. The height difference can be explained partly due to phototropism, competition for light among trees. However, it is more attributable to the excess water collected in the valleys and thicker rooting depth, which the trees growing there can utilise.

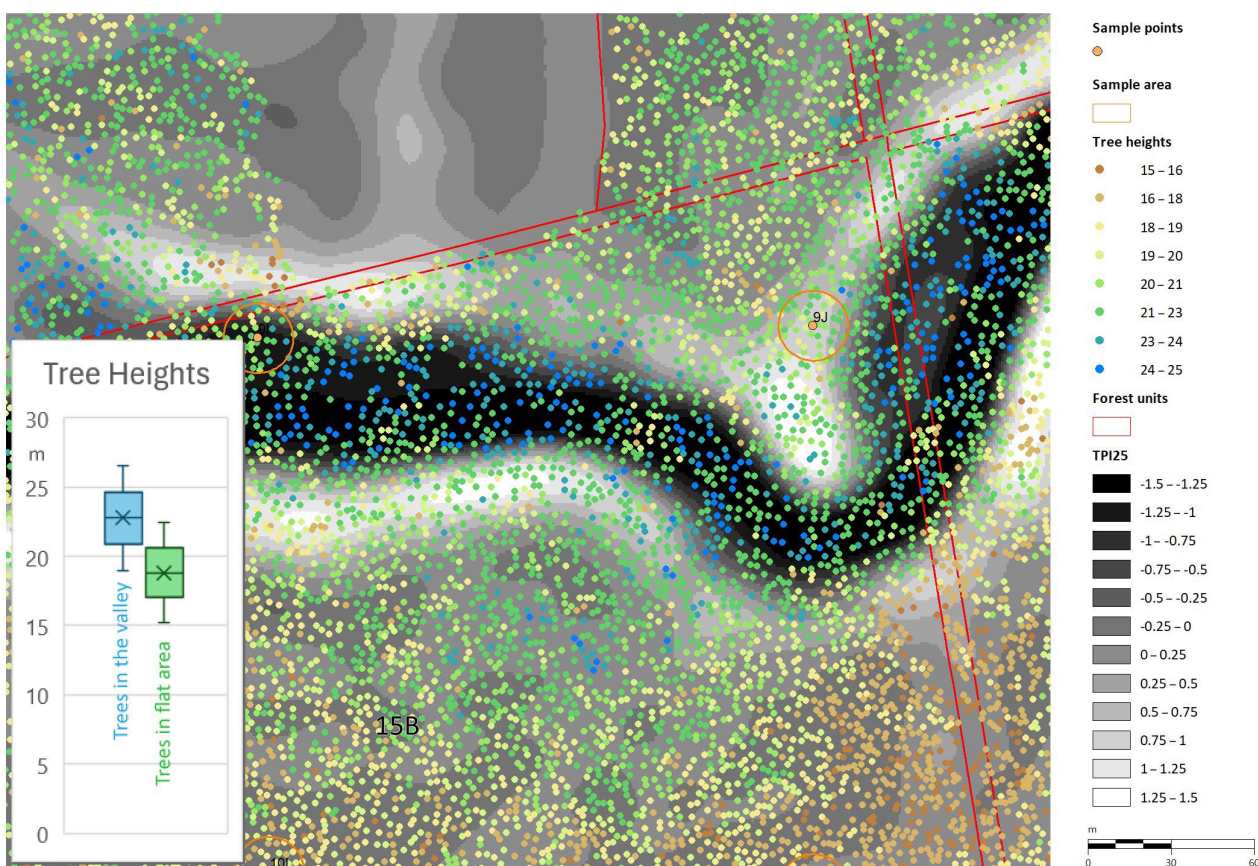


Figure 11. The tree heights (points) and the TPI25 map (raster) for forest subcompartment 15B, as well as the diagram of average tree heights (left side) in valleys and flat areas.

We also created a height yield map for the entire forested area, derived from the ratio of the CHM-based individual tree heights and the average age of the trees within each forest subcompartment. The results can be presented both on a map and in a chart. Based on the TPI25 raster, we formed groups (with a step size of 0.25) and calculated the average height increment within these groups. We found a strong correlation between the average values of TPI groups and height yield ($r^2 = 0.88$). This analysis clearly shows that lower TPI values are associated with greater height increments (Figure 12).

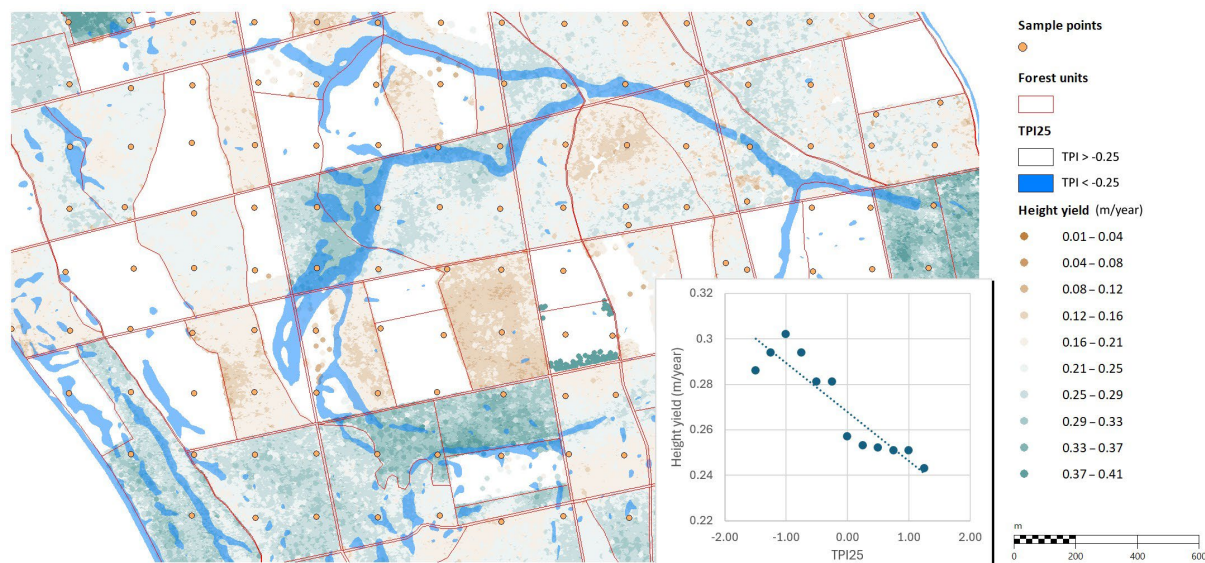


Figure 12. Height increment map, as well as the TPI25 and height increment relationship diagram.

4. Conclusions

Aerial laser scanning proves to be an excellent tool for mapping the topographic conditions of forest areas, including high-precision mapping of site conditions. Using the methods presented, various thematic layers can be derived from the elevation model, which allows for detailed, digital, objective, and automatable descriptions of forest site conditions. The TPI-based analyses involved deriving the applicable radius using mathematical methods. We examined the variability of topographic and orographic features within forest plots and their relationships between entropy and frequency.

The hierarchical morphological filtering algorithm used to generate the elevation model from the LiDAR data preserves even micro-topographical details. The model captures features such as forest roads and depressions caused by uprooted trees. These micro-elements can be filtered out, after which slope, aspect, TPI, and TPI with different radii can be determined. Such categorisation of terrain helps in creating site maps, selecting soil sampling locations, and even in the economic classification of forest areas.

Field GNSS RTK measurements validated the accuracy of the LiDAR elevation model, and field tree height measurements confirmed the accuracy of the LiDAR canopy height model.

We found significant correlations between the tree heights derived from LiDAR and the topographic position index (TPI) values within forest plots (in contrast to the study referenced as [49], where the findings indicated that the role of TPI was relatively small), as well as between the height increment map and the TPI map. These correlations are evident both in maps and graphs. The variability in tree heights within forest plots can be studied from various perspectives. Differences in tree height reflect the variability in terrain and soil. Already, we observe areas on the tree height and forest subcompartment maps where tree heights deviate from the average within the forest subcompartment. These deviations are likely due to varying soil parameters (such as shallower potential rooting depth, soil disturbance, different soil types, and consequently different water-holding capacities).

We carried out an in-depth site assessment at each of the 272 sampling points, including opening soil profile pits and collecting samples from various heights. The laboratory analysis of these samples is still in progress. Once the laboratory results are available, we plan to examine the relationships between the terrain and derived thematic layers, the single trees, and soil characteristics together.

Finally, it is worth emphasising that the goal of our research is to develop a new methodology for forest site mapping and carbon stock estimation supported by aerial remote sensing. As we continue to experience the rapid shift of site parameters, especially the climate and hydrology, this cost-effective, repeatable, yet precise and objective site

mapping method is valued more. All of this can assist professionals and decision makers with their management decisions.

Author Contributions: Conceptualisation, B.H., K.C. and G.K.; methodology, B.S. and K.C.; software, B.S. and K.C.; validation, G.V., D.M. and B.S.; formal analysis, D.H. and B.S.; investigation, B.S., G.V., G.I. and K.C.; resources, D.M. and G.I.; data curation, G.V., D.M., K.C. and B.S.; writing—original draft preparation, B.S. and K.C.; writing—review and editing, B.S., K.C. and D.H.; visualisation, B.S. and K.C.; supervision, G.I., D.H. and B.H.; project administration, D.M. and G.K.; funding acquisition, B.H., K.C. and G.K. All authors have read and agreed to the published version of the manuscript.

Funding: This research is supported by the Hungarian Ministry of Agriculture, State Secretariat for Forests and Land Affairs in the frame of Climate Change Action Plan, in the project “Digital Site-mapping and Carbon Stock Assessment in the Forest Soils of Hungary” (EGF/365/2023).

Data Availability Statement: The data that support the findings of this study are available from the corresponding authors upon reasonable request.

Acknowledgments: We thank the colleagues who participated directly and indirectly in this research for their support, especially the forest engineering students in the field measurement and the university colleagues in the procurement and administrative tasks.

Conflicts of Interest: The authors declare no conflicts of interest.

References

- Czimer, K.; Heil, B.; Illés, G.; Gribovszki, Z.; Veperdi, G.; Mészáros, D.; Szász, B.; Heilig, D.; Kovács, G. Korszerű távérzékelési, geoinformatikai, terepi referencia adatgyűjtési módszerekkel támogatott termőhely és szénkészlet térképezés (SoilSense). In Proceedings of the Forestry Scientific Conference, Sopron, Hungary, 5–6 February 2024; Abstract Volume, p. 9.
- Guth, P.L. Geomorphometry from SRTM. *Photogramm. Eng. Remote Sens.* **2006**, *72*, 269–277. [\[CrossRef\]](#)
- Mukherjee, S.; Joshi, P.K.; Mukherjee, S.; Ghosh, A.; Garg, R.D.; Mukhopadhyay, A. Evaluation of Vertical Accuracy of Open Source Digital Elevation Model (DEM). *Int. J. Appl. Earth Obs. Geoinf.* **2013**, *21*, 205–217. [\[CrossRef\]](#)
- Gallant, J.C. Primary Topographic Attributes. In *Terrain Analysis-Principles and Application*; Wilson, J.P., Gallant, J.C., Eds.; John Wiley & Sons: Hoboken, NJ, USA, 2000; pp. 51–86.
- Jain, S.K.; Singh, V.P. *Water Resources Systems Planning and Management*; Elsevier: Amsterdam, The Netherlands, 2023; p. 858, ISBN 978-0-323-98412-6.
- Chappell, N.A.; Vongtanaboon, S.; Jiang, Y.; Tangtham, N. Return-Flow Prediction and Buffer Designation in Two Rainforest Headwaters. *For. Ecol. Manag.* **2006**, *224*, 131–146. [\[CrossRef\]](#)
- Weibel, R.; Heller, M. A Framework for Digital Terrain Modeling. In Proceedings of the Fourth International Symposium on Spatial Data Handling, Zurich, Switzerland, 23–27 July 1990; pp. 219–229.
- Masataka, T. Accuracy of Digital Elevation Model According to Spatial Resolution. *Int. Arch. Photogramm. Remote Sens.* **1998**, *32*, 613–617.
- Abedini, M.J.; Dickinson, W.T.; Rudra, R.P. On Depressional Storages: The Effect of DEM Spatial Resolution. *J. Hydrol.* **2006**, *318*, 138–150. [\[CrossRef\]](#)
- Wolock, D.M.; Price, C.V. Effects of Digital Elevation Model Map Scale and Data Resolution on a Topography-Based Watershed Model. *Water Resour. Res.* **1994**, *30*, 3041–3052. [\[CrossRef\]](#)
- Zhang, W.; Montgomery, D.R. Digital Elevation Model Grid Size, Landscape Representation, and Hydrologic Simulations. *Water Resour. Res.* **1994**, *30*, 1019–1028. [\[CrossRef\]](#)
- Chisholm, H. *Encyclopedia Britannica: Ode-Payment of Members*; Cambridge: Cambridge, UK, 1911; Volume 20, p. 327.
- Weiss, A. Topographic Position and Landforms Analysis. In Proceedings of the Poster presentation, ESRI User Conference, San Diego, CA, USA, 9–13 July 2001; Volume 200.
- Jenness, J. Topographic Position Index (TPI). An ArcView 3. x Tool for Analyzing the Shape of the Landscape. 2006. Available online: https://www.jennessent.com/arcview/TPI_jen_poster.htm (accessed on 4 July 2024).
- Kraus, K.; Pfeifer, N. A new method for surface reconstruction from laser scanner data. *Int. Arch. Photogramm. Remote Sens.* **1997**, *32*, 80–86.
- Axelsson, P. DEM Generation from Laser Scanner Data Using Adaptive TIN Models, ISPRS—International Archives of the Photogrammetry. *Remote Sens. Spat. Inf. Sci.* **2000**, *33*, 110–117.
- Dong, Y.; Cui, X.; Zhang, L.; Ai, H. An Improved Progressive TIN Densification Filtering Method Considering the Density and Standard Variance of Point Clouds. *ISPRS Int. J. Geo-Inf.* **2018**, *7*, 409. [\[CrossRef\]](#)
- Vosselman, G. Slope based filtering of laser altimetry data. *Int. Arch. Photogramm. Remote Sens.* **2000**, *33*, 958–964.
- Pingel, T.; Clarke, K.; McBride, W.A. An Improved Simple Morphological Filter for the Terrain Classification of Airborne LIDAR Data. *ISPRS J. Photogramm. Remote Sens.* **2013**, *77*, 21–30. [\[CrossRef\]](#)

20. Zhang, K.; Chen, S.; Whitman, D.; Shyu, M.; Yan, J.; Zhang, C. A progressive morphological filter for removing nonground measurements from airborne LIDAR data. *IEEE Trans. Geosci. Remote Sens.* **2003**, *41*, 872–882. [[CrossRef](#)]
21. Evans, J.S.; Hudak, A.T. A Multiscale Curvature Algorithm for Classifying Discrete Return LiDAR in Forested Environments. *IEEE Trans. Geosci. Remote Sens.* **2007**, *45*, 1029–1038. [[CrossRef](#)]
22. Meng, X.; Currit, N.; Zhao, K. Ground Filtering Algorithms for Airborne LiDAR Data: A Review of Critical Issues. *Remote Sens.* **2010**, *2*, 833–860. [[CrossRef](#)]
23. Cai, S.; Zhang, W.; Liang, X.; Wan, P.; Qi, J.; Yu, S.; Yan, G.; Shao, J. Filtering Airborne LiDAR Data through Complementary Cloth Simulation and Progressive TIN Densification Filters. *Remote Sens.* **2019**, *11*, 1037. [[CrossRef](#)]
24. Li, F.; Zhu, H.; Luo, Z.; Shen, H.; Li, L. An Adaptive Surface Interpolation Filter Using Cloth Simulation and Relief Amplitude for Airborne Laser Scanning Data. *Remote Sens.* **2021**, *13*, 2938. [[CrossRef](#)]
25. Hyypä, J.; Kelle, O.; Lehikoinen, M.; Inkinen, M. A segmentation-based method to retrieve stem volume estimates from 3-D tree height models produced by laser scanners. *IEEE Trans. Geosci. Remote Sens.* **2001**, *39*, 969–975. [[CrossRef](#)]
26. Persson, A.; Holmgren, J.; Söderman, U. Detecting and measuring individual trees using an airborne laser scanner. *Photogramm. Eng. Remote Sens.* **2002**, *68*, 925–932.
27. Popescu, S.C.; Wynne, R.H. Seeing the trees in the forest: Using lidar and multispectral data fusion with local filtering and variable window size for estimating tree height. *Photogramm. Eng. Remote Sens.* **2004**, *70*, 589–604.
28. Morsdorf, F.; Meier, E.; Kötz, B.; Itten, K.I.; Dobbertin, M.; Allgöwer, B. LIDAR-based geometric reconstruction of boreal type forest stands at single tree level for forest and wildland fire management. *Remote Sens. Environ.* **2004**, *92*, 353–362. [[CrossRef](#)]
29. Chen, Q.; Baldocchi, D.; Gong, P.; Kelly, M. Isolating Individual Trees in a Savanna Woodland using Small Footprint LIDAR data. *Photogramm. Eng. Remote Sens.* **2006**, *72*, 923–932. [[CrossRef](#)]
30. Koch, B.; Heyder, U.; Weinacker, H. Detection of individual tree crowns in airborne lidar data. *Photogramm. Eng. Remote Sensing* **2006**, *72*, 357–363. [[CrossRef](#)]
31. Hyypä, J.; Hyypä, H.; Yu, X.; Kaartinen, H.; Kukko, A.; Holopainen, M. Forest Inventory Using Small-Footprint Airborne Lidar. In *Topographic Laser Ranging and Scanning: Principles and Processing*; Shan, J., Toth, C.K., Eds.; Taylor & Francis Group: New York, NY, USA, 2009; pp. 335–370.
32. Lee, H.; Slatton, K.C.; Roth, B.E.; Cropper, W.P. Adaptive clustering of airborne LiDAR data to segment individual tree crowns in managed pine forests. *Int. J. Remote Sens.* **2010**, *31*, 117–139. [[CrossRef](#)]
33. Ferraz, A.; Bretar, F.; Jacquemoud, S.; Gonçalves, G.; Pereira, L.; Tomé, M.; Soares, P. 3-D mapping of a multi-layered Mediterranean forest using ALS data. *Remote Sens. Environ.* **2012**, *121*, 210–223. [[CrossRef](#)]
34. Li, W.K.; Guo, Q.H.; Jakubowski, M.K.; Kelly, M. A new method for segmenting individual trees from the lidar point cloud. *Photogramm. Eng. Remote Sens.* **2012**, *78*, 75–84. [[CrossRef](#)]
35. Kaartinen, H.; Hyypä, J.; Yu, X.; Vastaranta, M.; Hyypä, H.; Kukko, A.; Holopainen, M.; Heipke, C.; Hirschmugl, M.; Morsdorf, F.; et al. An International Comparison of Individual Tree Detection and Extraction Using Airborne Laser Scanning. *Remote Sens.* **2012**, *4*, 950–974. [[CrossRef](#)]
36. Jakubowski, M.K.; Li, W.; Guo, Q.; Kelly, M. Delineating Individual Trees from Lidar Data: A Comparison of Vector- and Raster-based Segmentation Approaches. *Remote Sens.* **2013**, *5*, 4163–4186. [[CrossRef](#)]
37. Strimbu, V.F.; Strimbu, B.M. A graph-based segmentation algorithm for tree crown extraction using airborne LiDAR data. *ISPRS J. Photogramm. Remote Sens.* **2015**, *104*, 30–43. [[CrossRef](#)]
38. Duncanson, L.I.; Cook, B.D.; Hurtt, G.C.; Dubayah, R.O. An efficient, multi-layered crown delineation algorithm for mapping individual tree structure across multiple ecosystems. *Remote Sens. Environ.* **2014**, *154*, 378–386. [[CrossRef](#)]
39. Yang, B.; Dai, W.; Dong, Z.; Liu, Y. Automatic Forest Mapping at Individual Tree Levels from Terrestrial Laser Scanning Point Clouds with a Hierarchical Minimum Cut Method. *Remote Sens.* **2016**, *8*, 372. [[CrossRef](#)]
40. Lindberg, E.; Holmgren, J. Individual tree crown methods for 3D data from remote sensing. *Curr. For. Rep.* **2017**, *3*, 19–31. [[CrossRef](#)]
41. Hu, S.; Li, Z.; Zhang, Z.; He, D.; Wimmer, M. Efficient tree modeling from airborne LiDAR point clouds. *Comput. Graph.* **2017**, *67*, 1–13.
42. Ayrey, E.; Fraver, S.; Kershaw, J.A., Jr.; Kenefic, L.S.; Hayes, D.; Weiskittel, A.R.; Roth, B.E. Layer Stacking: A Novel Algorithm for Individual Forest Tree Segmentation from LiDAR Point Clouds. *Can. J. Remote Sens.* **2017**, *43*, 16–27. [[CrossRef](#)]
43. Wan Mohd Jaafar, W.S.; Woodhouse, I.H.; Silva, C.A.; Omar, H.; Abdul Maulud, K.N.; Hudak, A.T.; Klauber, C.; Cardil, A.; Mohan, M. Improving Individual Tree Crown Delineation and Attributes Estimation of Tropical Forests Using Airborne LiDAR Data. *Forests* **2018**, *9*, 759. [[CrossRef](#)]
44. Wang, Y.; Lin, Y.; Cai, H.; Li, S. Hierarchical Fine Extraction Method of Street Tree Information from Mobile LiDAR Point Cloud Data. *Appl. Sci.* **2023**, *13*, 276. [[CrossRef](#)]
45. Czimmer, K. Forest inventory with aerial laser scanning and near photogrammetry—First test results (in Hungarian: Erdőleltározás légi lézeres letapogatással és közel fotogrammetriával—Első tesztek eredményei). In Proceedings of the Theory meets practice in GIS Conference, Debrecen, Hungary, 23–24 March 2019; pp. 77–81.
46. McNab, W.H. Terrain Shape Index: Quantifying Effect of Minor Landforms on Tree Height. *For. Sci.* **1989**, *35*, 91–104. [[CrossRef](#)]
47. Tateno, R.; Takeda, H. Forest Structure and Tree Species Distribution in Relation to Topography-Mediated Heterogeneity of Soil Nitrogen and Light at the Forest Floor. *Ecol. Res.* **2003**, *18*, 559–571. [[CrossRef](#)]

48. Rahman, F.M.; Onoda, Y.; Kitajima, K. Forest Canopy Height Variation in Relation to Topography and Forest Types in Central Japan with LiDAR. *For. Ecol. Manag.* **2022**, *503*, 119792. [[CrossRef](#)]
49. Bałazy, R.; Kamińska, A.; Ciesielski, M.; Socha, J.; Pierzchalski, M. Modeling the Effect of Environmental and Topographic Variables Affecting the Height Increment of Norway Spruce Stands in Mountainous Conditions with the Use of LiDAR Data. *Remote Sens.* **2019**, *11*, 2407. [[CrossRef](#)]
50. Dövényi, Z.; Becse, A. *Magyarország Kistájainak Katasztere. Második, Átdolgozott És Bővített Kiadás*; MTA Földrajztudományi Kutint: Budapest, Hungary, 2010; pp. 347–350.
51. Karaca, Y.; Moonis, M. Chapter 14—Shannon Entropy-Based Complexity Quantification of Nonlinear Stochastic Process: Diagnostic and Predictive Spatiotemporal Uncertainty of Multiple Sclerosis Subgroups. In *Multi-Chaos, Fractal and Multi-Fractional Artificial Intelligence of Different Complex Systems*; Karaca, Y., Baleanu, D., Zhang, Y.-D., Gervasi, O., Moonis, M., Eds.; Academic Press: Cambridge, MA, USA, 2022; pp. 231–245, ISBN 978-0-323-90032-4.

Disclaimer/Publisher’s Note: The statements, opinions and data contained in all publications are solely those of the individual author(s) and contributor(s) and not of MDPI and/or the editor(s). MDPI and/or the editor(s) disclaim responsibility for any injury to people or property resulting from any ideas, methods, instructions or products referred to in the content.